EPJ Web of Conferences **95**, 01012 (2015)
DOI: 10.1051/epjconf/ 20159501012

Search for exotics at *BABAR*

Elisabetta Prencipe[1,2,a] on behalf of the *BABAR* Collaboration.

[1] *Forschungszentrum Jülich, Leo Brandt strasse, 52428 Jülich, Germany*
[2] *Previously addressed at the Johannes Gutenberg University of Mainz, Germany*

Abstract. One of the most intriguing puzzles in hadron spectroscopy are the numerous charmonium-like states observed in the last decade, including charged states that are manifestly exotic. Over the years, the experiment *BABAR* has extensively studied those in B meson decays, initial state radiation processes and two photon reactions. We report in this paper new and additional studies on some of those states, performed using the entire data sample collected by *BABAR* in e^+e^- collisions, at center of mass energies near 10.58 GeV/c^2. Among these, the study of the process $B \to J/\psi\phi K$, with a search for the resonant states X(4140) and X(4270) in their decays to $J/\psi\phi$, will be highlighted. The recent *BABAR* results of the Dalitz analysis of η_c to 3 pseudoscalar mesons, via 2-photon interactions, will be also presented in this report. Preliminary results on χ_{bJ} in the field of bottomonium spectroscopy will be introduced.

1 Analysis of the decay $B \to J/\psi KKK$

1.1 Motivation

Several new Charmonium-like states have been observed at *BABAR*, revealing a spectrum too rich to be uniquely described by potential models[1]. Different hypotheses have been proposed from theorists to explain their nature, such as hybrid charmonium states, diquark-antidiquark states or $D^0\bar{D}^{0(*)}$ molecules[2]. While resonant structures like the X(3872) have been seen in $B \to XK, X \to J/\psi\,\pi^+\pi^-$, or like Y(4260) by investigating the process $e^+e^- \to \gamma_{ISR}X$, $X \to J/\psi\pi^+\pi^-$[3–5], no indication of new states has been observed in the $J/\psi\ K^+K^-$ invariant mass system, until the paper quoted in Ref. [6] highlighted the possibility of a couple of resonant states, decaying to $J/\psi\phi$, with $\phi \to K^+K^-$ and $J/\psi \to \mu^+\mu^-$. These observations are nowaday controversial.

Strangeness in charmonium seems a sector still to be exploited. In this context, the analysis performed by *BABAR* on $B \to J/\psi KKK$, and in particular $B \to J/\psi\phi K$, could have important impact in understanding the puzzle of the Charmonium spectroscopy. The rare decay $B \to J/\psi\phi K$ is interesting because it is a promising place to search for new resonances, as it proceeds, at quark level, via the weak transition $b \to c\bar{c}s$ (Fig. 1). It could be a quasi 2-body decay, $B \to X_gK$, with $X_g \to J/\psi\phi$, where $X_g = |gc\bar{c}s\bar{s}>$, with gluonic contribution (g). The QCD spectrum is much richer than that of the naive quark model, as the gluons, which mediate the strong force between quarks, can also act as principal components of entirely new types of hadrons. These gluonic hadrons fall into two general categories: glueballs and hybrids.

[a] e-mail: e.prencipe@fz-juelich.de

Table 1. BF values of light mesons decaying to K^+K^- as reported in [9], with BF>1%.

Decay channel	BF (%)	J^G (J^{PC})
$a_0(980) \to K^+K^-$	seen	$1^-(0^{++})$
$f_0(980) \to K^+K^-$	seen	$0^+(0^{++})$
$\phi(1020) \to K^+K^-$	48.9 ± 0.5	$0^-(1^{--})$
$f_2(1270) \to K^+K^-$	4.6 ± 0.4	$0^+(2^{++})$
$a_2(1320) \to K^+K^-$	4.9 ± 0.8	$1^-(2^{++})$
$f_2^{'}(1525) \to K^+K^-$	88.8 ± 3.1	$0^+(2^{++})$
$\phi(1680) \to K^+K^-$	seen	$0^-(1^{--})$

Glueballs are excited states of pure glue, while hybrids are resonances consisting largely of a quark, an antiquark, and excited glue. The additional degrees of freedom carried by gluons allow glueballs and hybrids to have spin-exotic quantum numbers J^{PC} that are forbidden for normal mesons and other fermion-antifermion systems. Exotic quantum numbers (e.g. 0^{--}, 0^{+-}, 1^{-+}, 2^{+-}) are the easiest way to distinguish gluonic hadrons from $q\bar{q}$ states. In the specific case described in this document, we are looking for possible resonant states decaying to two mesons: J/ψ, and another meson (e.g. we can call it H_s) with strange s-quark content, decaying to 2 kaons, as reported in Table 1. In the next sections the particular case of $H_s = \phi$, $\phi \to K^+K^-$, is detailed examinated. Exotic quantum number combinations are theoretically allowed, in this case. Predictions for hybrids come mainly from calculations based on the bag model, flux tube model, and constituent gluon model and recently, with increasing precision, from Lattice QCD. All these calculations do quite well in predicting the properties of the already known $q\bar{q}$ states, where q = heavy quark. The quark s is a border-case between light and heavy quarks, and it makes complicated theoretical calculations.

The decay of the hybrid candidates X_g into $J/\psi\phi$ would be however observable below 4.3 GeV/c^2; above this threshold, the DD^{**} branching ratio largely dominates other modes.

Using 56 million $B\bar{B}$ pairs, in 2003 *BABAR* set up the branching fractions (BF) for the decay $B^{\pm,0} \to J/\psi\phi K^{\pm,0}$[7], not in good agreement with the previous *CLEO*-II first measurements[8]. Fig. 1 shows the possible Feynman diagrams of the physics processes under study. This paper presents a new determination of the BF of $B^{\pm,0} \to J/\psi K^+K^-K^{\pm,0}$ and $B^{\pm,0} \to J/\psi\phi K^{\pm,0}$, using eight times more data than that reported in the PDG[7]. A study of the $J/\psi\phi$ invariant mass spectrum is later reported, together with the invariant mass study of the $J/\psi K$ and the KKK invariant mass systems. The upper limit (UL) of the decay $B^0 \to J/\psi\phi$ is also presented.

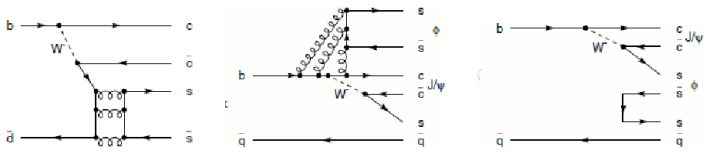

Figure 1. Rescattering diagrams for $B^0 \to J/\psi\phi$ (left); quark diagrams for $B \to J/\psi\phi K$ via strange sea quarks (central) and gluon coupling (right).

1.2 Analysis strategy

The analysis $B^+ \to J/\psi K^+K^-K^+$, $B^0 \to J/\psi K^+K^-K_S^0$, $B^+ \to J/\psi\phi K^+$, $B^0 \to J/\psi\phi K_S^0$ and $B^0 \to J/\psi\phi$ are performed using 469 million $B\bar{B}$ pairs collected by *BABAR* at the energy in the center of

Table 2. BF measurements for the 3-body and 2-body final states. The yields are efficiency-corrected.

B channel	Corrected yield ($\bar{\epsilon}$)	Corrected yield (ϵ_D)	BF ($\times 10^{-5}$) calculated with $\bar{\epsilon}$	BF ($\times 10^{-5}$) calculated with ϵ_D
$B^+ \to J/\psi\phi K^+$	1161± 86	1396±103	4.21±0.31 (stat)	5.06±0.37(stat)±0.15(sys)
$B^0 \to J/\psi\phi K^0_S$	382± 65	406± 69	2.00±0.34 (stat)	2.13±0.36(stat)±0.06(sys)
$B^0 \to J/\psi\phi$	19 ± 13		< 0.101	

mass of 10.56 GeV. With B^+ we will imply in the text also the charged conjugate B^-.
B^+ candidates are reconstructed by combining the J/ψ candidate, reconstructed to e^+e^- and $\mu^+\mu^-$, with three loosely identified kaons and require a vertex probability larger than 0.1%. J/ψ is then mass constraint. Similarly, for $B^0 \to J/\psi K^- K^+ K^0_S$ candidates, we combine the J/ψ and K^0_S with two loosely identified kaons and require a vertex probability larger than 0.1%. A K^0_S candidate is formed by geometrically constraining a pair of oppositely charged tracks to a common vertex, with χ^2 fit probability larger than 0.1%. K^0_S is reconstructed to $\pi^+\pi^-$. We further select B meson candidates using the energy difference $\Delta E = E^*_B - \sqrt{s}/2$ in the center-of-mass (c.m.) frame and the beam-energy-substituted mass defined as $m_{ES} = \sqrt{((s/2 + \vec{p}_i \cdot \vec{p}_B)/E_i)^2 - \vec{p}^{\,2}_B}$, where $(E_i, \vec{p}_i)$ is the initial state e^+e^- four-momentum vector in the laboratory frame and $\sqrt{s}$ is the c.m. energy. In the above expressions E^*_B is the B meson candidate energy in the c.m. frame, and $\vec{p}_B$ is its laboratory frame momentum. When multiple candidates are present, the combination with the smallest ΔE is chosen. The final selection requires $|\Delta E| < 30$ MeV and $|\Delta E| < 25$ MeV for B^+ and B^0 decays, respectively; the selection criterion m_{ES} >5.2 GeV/c^2 is required for the calculation of the BFs, while m_{ES} >5.27 GeV/c^2 is applied to select the signal region for the analysis of the invariant mass systems.

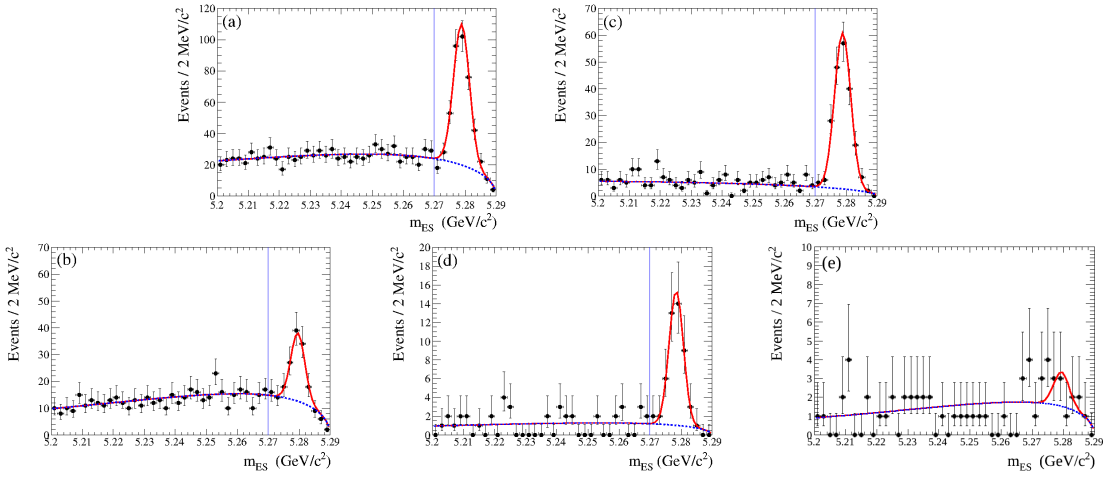

Figure 2. The m_{ES} distributions for (a) $B^+ \to J/\psi K^+ K^- K^+$, (b) $B^+ \to J/\psi\phi K^+$, (c) $B^0 \to J/\psi K^- K^+ K^0_S$, (d) $B^0 \to J/\psi\phi K^0_S$ and (e) $B^0 \to J/\psi\phi$ for the ΔE regions indicated in the text. The continuous (red) curve represents the signal plus background, while the dotted (blue) curve represents the fitted background. Vertical (blue) lines indicate the selected signal regions.

An unbinned maximum likelihood fit is performed to m_{ES} to extract the yield and calculate the BFs, as reported in Table 2, and shown in Fig. 2. The m_{ES} fit is performed using a gaussian function to parametrize the signal, and ARGUS function for the backround. The secondary BFs of $J/\psi \to l^+l^-$ (l = lepton, e or μ), $\phi \to K^+K^-$, $K^0_S \to \pi^+\pi^-$ are taken from [9]. The $\phi(1020)$ signal region is selected in the mass range [1.004; 1.034] GeV/c^2. The average efficiency ($\bar{\epsilon}$) is evaluated as reconstruced over generated events. The Dalitz efficiency (ϵ_D) is evaluated dividing reconstructed over generated events of the Dalitz plot $m^2_{J/\psi\phi}$ vs $m^2_{\phi K}$. BFs are calculated dividing the efficiency-corrected yield over the product of $N_{B\bar{B}}$ * secondary BFs of the other particles involved in the decay process. For the 4-body decays $B^+ \to J/\psi K^+K^-K^+$ and $B^0 \to J/\psi K^+K^-K^0_S$ we used the average efficiency, due to the difficulty to perform a Dalitz plot analysis with a 4-body decay, and because of the presence of the background in the signal area, difficult to parametrize. For the 3-body decays $B \to J/\psi\phi K$ we compare in Table 2 two methods for the BF calculation: efficiency-correction performed with $\bar{\epsilon}$ and efficiency-correction with ϵ_D. We consider correct the second, because the correction is properly done event by event using information from the Dalitz plot. The differences with the 2 methods for the BF calculations are due to the efficiency loss at the threshold of the invariant mass distribution $J/\psi\phi$, as reported later. These results are preliminary. A detailed explanation on the BF systematic effects is reported in Ref. [13], together with the relevant discussion concerning the K^+K^- non-resonant contribution to the $\mathcal{B}(B \to J/\psi KKK)$. We also calculate: $R_\phi = \mathcal{B}(B^0 \to J/\psi\phi K^0_S)/\mathcal{B}(B^+ \to J/\psi\phi K^+)$ = 0.48 ± 0.09 ± 0.02 , and $R_{2K} = \mathcal{B}(B^0 \to J/\psi K^+K^-K^0_S)/\mathcal{B}(B^+ \to J/\psi K^+K^-K^+)$ = 0.52 ± 0.09 ± 0.03; we find those in agreement with the expectation of the spectator quark model (e.g., R~0.5).

The study of the invariant mass systems $J/\psi KK$, $J/\psi K$ and KKK is then performed. We plot in Fig. 3(a) the $J/\psi K^+K^-$ mass distributions for $B^+ \to J/\psi K^+K^-K^+$ and in Fig. 3(b) that for $B^0 \to J/\psi K^-K^+K^0_S$; the signal regions are defined by the ΔE selections indicated in the text and m_{ES} >5.27 GeV/c^2. No prominent structure is observed in both mass spectra.

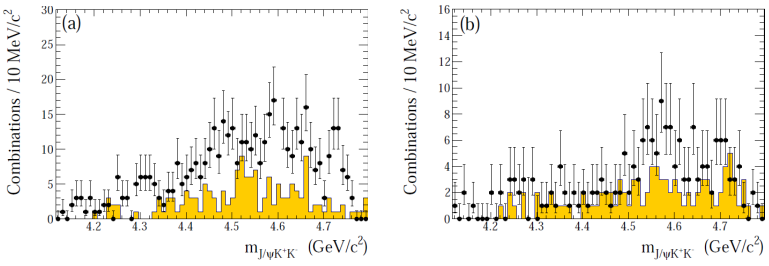

Figure 3. Invariant mass distribution of $J/\psi K^+K^-$ for (a) $B^+ \to J/\psi K^-K^+K^+$ and (b) $B^0 \to J/\psi K^-K^+K^0_S$. ΔE sidebands, describing the background of these 2 invariant mass systems, are shown in yellow (shaded histograms).

We search for the resonant states reported by the CDF Collaboration in the $J/\psi\phi$ mass spectrum. The masses and the widths are fixed to m=4143.4 MeV/c^2 and Γ=15.3 MeV for the $X(4140)$, and m=4274.4 MeV/c^2 and Γ= 32.3 MeV for the X(4270) resonance, according to Ref. [6]. We first evaluate the mass resolution using MC simulations and obtain 2 MeV/c^2 resolution in the mass region between 4100 MeV/c^2 and 4300 MeV/c^2. Therefore resolution effects can be ignored because they are much smaller than the widths of the resonances under consideration.

We observed significant efficiency decrease at low $J/\psi\phi$ mass, due to the inability to reconstruct slow kaons in the laboratory frame, as a result of energy loss in the beampipe and SVT material. We perform an unbinned maximum likelihood fit to the channel $B^+ \to J/\psi\phi K^+$. We model the resonances using S-wave relativistic Breit-Wigner (BW) functions with parameters fixed to the CDF values [6]. A

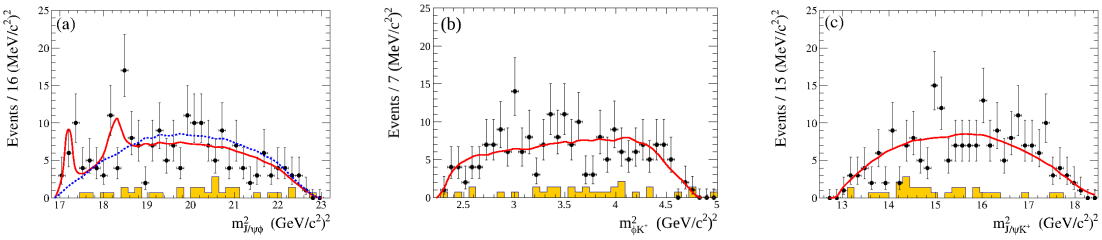

Figure 4. Dalitz plot projections for $B^+ \to J/\psi\phi K^+$ on (a) $m^2_{J/\psi\phi}$, (b) $m^2_{\phi K^+}$, and (c) $m^2_{J/\psi K^+}$. The continuous (red) curves are the results from fit model A performed including the $X(4140)$ and $X(4270)$ resonances. The dashed (blue) curve in (a) indicates the projection for fit model D, with no resonances. The shaded (yellow) histograms indicate the background estimated from the ΔE sidebands.

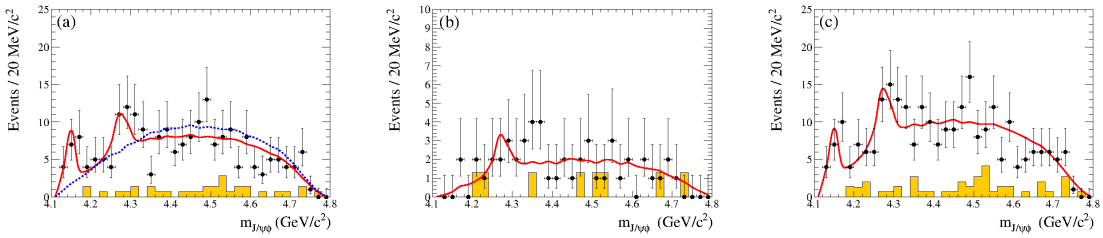

Figure 5. Projections on the $J/\psi\phi$ mass spectrum from the Dalitz plot fit with the $X(4140)$ and the $X(4270)$ resonances for the (a) B^+, (b) B^0, and (c) combined B^+ and B^0 data samples. The continuous (red) curves result from the fit; the dashed (blue) curve in (a) indicates the projection for fit model D, with no resonances. The shaded (yellow) histograms show the background contributions estimated from the ΔE sidebands.

non-resonant contribution is described according to PHSP. The 2 BWs are inchoerent with each other, and with the non-resonant PHSP contribution. The background contributions estimated from the ΔE sidebands are small and are consistent with the PHSP behavior, so in the fit they are incorporated into the non-resonant PHSP term. The decay of a pseudoscalar meson to two vector states contains high spin contributions which could generate non-uniform angular distributions. However, due to the limited data sample we do not include such angular terms, and assume that the resonances decay isotropically. The amplitudes are normalized using PHSP MC generated events with B parameters obtained from the fit to the data. The fit function is weighted by the inverse of the two-dimentional efficiency computed on the Dalitz plots. We perform fits separately for the charged B^+ sample and the combined B^+ and B^0 one. Due to the very limited statistics of the B^0 sample we do not perform a separate fit, but we subtract the fit to the B^+ sample from the fit to the combined B^+ and B^0 sample (see Fig. 4 and Fig. 5.). Table 3 summarizes the results from the fits to the data. In the table we report the fractions of the two resonances, $f_{X(4140)}$ and $f_{X(4270)}$, the two-dimensional (2D) χ^2 computed on the Dalitz plot and the one-dimensional (1D) χ^2 computed on the $J/\psi\phi$ mass projection. We perform the fits using models with two resonances (labeled model A), one resonance (models B and C), and no resonances (model D). The fit projections for fit A are displayed in Fig. 5 and fit results are summarized in Table 3. All models provide a reasonably good description of the data, with χ^2

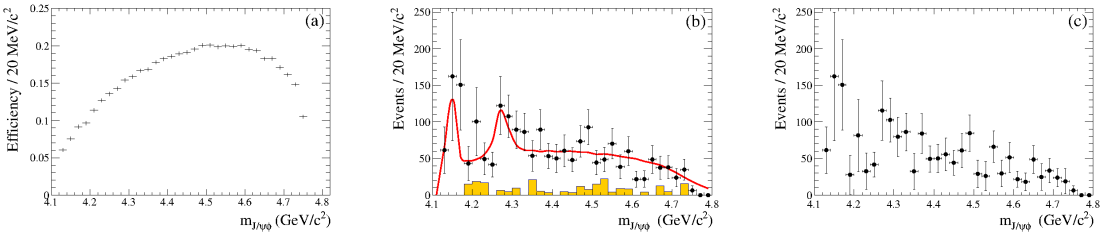

Figure 6. Dalitz plot projections for $B^+ \to J/\psi\phi K^+$ on (a) $m^2_{J/\psi\phi}$, (b) $m^2_{\phi K^+}$, and (c) $m^2_{J/\psi K^+}$. The continuous (red) curves are the results from fit model A performed including the $X(4140)$ and $X(4270)$ resonances. The dashed (blue) curve in (a) indicates the projection for fit model D, with no resonances. The shaded (yellow) histograms indicate the background estimated from the ΔE sidebands.

Table 3. Fits to the $B \to J/\psi\phi K$ Dalitz plot. For each fit, the table gives the fit fraction for each resonance, and the 2D and 1D χ^2 values. The fractions are corrected for the background component as explained in the text.

Channel	Fit	$f_{X(4140)}(\%)$	$f_{X(4270)}(\%)$	2D χ^2/ν	1D χ^2/ν
B^+	A	9.2 ± 3.3	10.6 ± 4.8	12.7/12	6.5/20
	B	9.2 ± 2.9	0.	17.4/13	15.0/17
	C	0.	10.0 ± 4.8	20.7/13	19.3/19
	D	0.	0.	26.4/14	34.2/18
$B^0 + B^+$	A	7.3 ± 3.8	12.0 ± 4.9	8.5/12	15.9/19

probability larger than 5%. We estimate systematic errors on the fractions by varying the masses and the widths of both resonances within their uncertainties. The results shown in Table 3 are corrected by the fraction of background estimated in the sample, which corresponds to a correction factor of 1.12 and 1.21 for the B^+ and the B^0 channels, respectively. We obtain the following corrected-estimates for the fractions for B^+, where the central values of mass and width of the two resonances are fixed to the values recently published from CDF[6] (Eq. 1) and CMS [10] (Eq. 2), respectively:

$$f_{X(4140)} = (9.2 \pm 3.3 \pm 4.7)\%,\ f_{X(4270)} = (10.6 \pm 4.8 \pm 7.1)\%. \quad (1)$$

$$f_{X(4140)} = (13.2 \pm 3.8 \pm 6.8)\%,\ f_{X(4270)} = (10.9 \pm 5.2 \pm 7.3)\%. \quad (2)$$

These values are consistent within the uncertainties. For comparison, CMS reported a fraction of 0.10 ± 0.03 for the X(4140), compatible with CDF, LHCb and our values within the uncertainties. CMS could not determine reliably the significance of the second structure X(4270) due to possible reflections of two-body decays. Using the Feldman-Cousins method [11], we obtain the ULs at 90% CL:

$$BF(B^+ \to X(4140)K^+) \times BF(X(4140) \to J/\psi\phi)/BF(B^+ \to J/\psi\phi K^+) < 0.135 \quad (3)$$

$$BF(B^+ \to X(4270)K^+) \times BF(X(4270) \to J/\psi\phi)/BF(B^+ \to J/\psi\phi K^+) < 0.184. \quad (4)$$

The Feldman-Cousin intervals are evaluated as explained in Ref. [11]. The $X(4140)$ limit may be compared with the CDF measurement of $0.149 \pm 0.039 \pm 0.024$ [6] and the LHCb limit of 0.07 [12]. The

$X(4270)$ limit may be compared with the LHCb limit of 0.08. In Fig. 6(a) we show the dependence on $J/\psi\phi$ mass of the efficiency obtained from the MC generator, according to PHSP. An efficiency-corrected version of Fig. 5(c) is obtained by using the 2D-efficiency map to assign an efficiency value (ϵ_i) to the $i-th$ event, giving it as weight $1/\epsilon_i$, and forming the weighted distribution shown in Fig. 6(b). In each mass interval of Fig. 6(b) the ordinate is the sum of the weights and its uncertainty is given by the square root of the sum of the squared weights. We then add the new efficiency-corrected plots of B^+ and B^0 data sample, and fit the resulting distribution shown in Fig. 6(b), which represents an efficiency-corrected version of the plot of Fig. 5(c). The fit function is obtained by adding PHSP plus 2 inchoerent relativistic BWs, as for the fit of Fig. 5(c), where the only free parameters of the fit are the yields of the 2 peaks. Non significant evidence of the 2 peaks labeled as the $X(4140)$ and the $X(4270)$ is found on 424 fb^{-1} integrated luminosity in B decays: we found respectively 1.2 and 1.6σ significance only, including systematic effects. A comparison among the re-weighted and background-subtracted points of Fig. 6(c) and the other experiment results, scaled by the proper factor, re-binned in a consistent way and background-corrected, is shown in Fig. 7. A detailed description

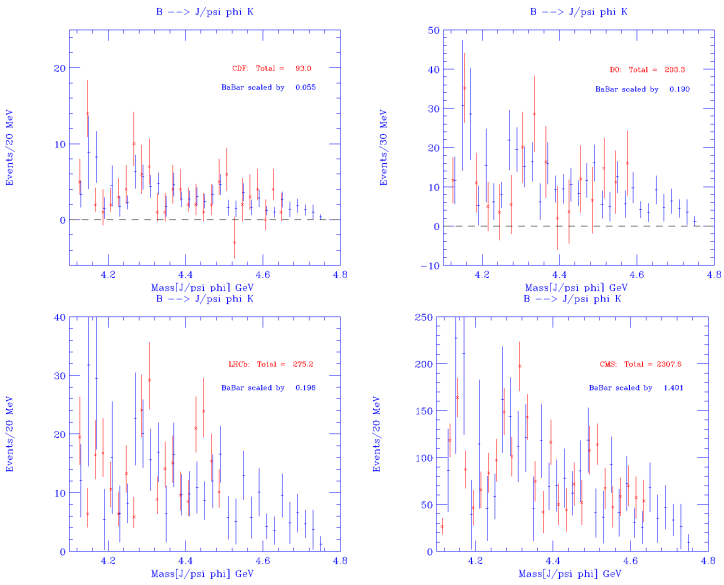

Figure 7. Comparison between the BaBar results and those published by CDF (top-left), D0 (top-right), LHCb (down-left), and CMS (down-right). Informations are taken from Ref. [6, 10, 12–14].

of all BFs and ULs shortly introduced in this report is in Ref. [13]: this work has been submitted to PRD.

2 Decay of η_c to 3 pseudoscalar mesons via 2-photon interactions.

2.1 Motivation

Charmonium decays, in particular J/ψ radiative and hadronic decays, have been studied extensively[15]. One of the motivations for these studies is the search for non-$q\bar{q}$ mesons such as glueballs or molecular states that are predicted by QCD to populate the low mass region of the hadron

mass spectrum[16]. Recently, a search for exotic resonances was performed through Dalitz plot analyses of χ_{c1} states[17]. Scalar mesons are still a puzzle in light-meson spectroscopy, as there are too many states and they are not consistent with the quark model. In particular, the $f_0(1500)$ resonance, discovered in $\bar{p}p$ annihilations, has been interpreted as a scalar glueball[18]. However, no evidence for the $f_0(1500)$ state has been found in charmonium decays. Another glueball candidate is the $f_0(1710)$ discovered in radiative J/ψ decays. Recently, $f_0(1500)$ and $f_0(1710)$ signals have been incorporated in a Dalitz plot analysis of $B \to 3K$ decays[19]. Charmless $B \to XK$ could enanche gluonium production[20]. Another puzzling state is the $K_0^*(1430)$, never observed as clear peak in $K\pi$ invariant mass. Its parameters were measured from the LASS experiment in $K^- p \to K^-\pi^+ n$[21].

The Dalitz analysis here summarized, $\eta_c \to K^+K^-\eta/\pi^0$ via 2-photon interactions, is relevant to several issues in light meson spectroscopy, and it is recently published by *BABAR*[22]. No Dalitz plot analysis has been performed on η_C three-body decays until now.

2.2 Analysis strategy

We describe a study of the decays $\eta_c \to K^+K^-\eta$ and $\eta_c \to K^+K^-\pi^0$, with $\eta \to \pi^+\pi^-\pi^0$, $\eta \to \gamma\gamma$ and $\pi^0 \to \gamma\gamma$, produced in two-photon interactions. The data sample used is 519 fb^{-1} at *BABAR*. Two-photon events in which at least one of the interacting photons is not quasireal are strongly suppressed by a dedicated selection. This implies that the allowed J^{PC} values of any produced resonances are $0^{\pm,+}$, $2^{\pm,+}$, $3^{+,+}$, $4^{+,+}$,...[24].

A clear peak of η_c is seen, and well reconstructed in the invariant mass systems of $K^+K^-\eta$ and $K^+K^-\pi^0$ (see Fig. 8(a, b)). All decay modes under exam are summarized in Table 4, with the

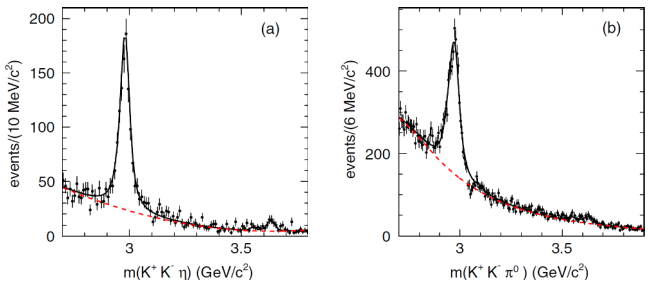

Figure 8. (a) The $K^+K^-\eta$ mass spectrum summed over the two η decay modes. (b) The $K^+K^-\pi^0$ mass spectrum. The solid curve represents the total fit function, the dashed curve shows the fitted background contribution.

parameters measured from the fit. A summary of the results obtained in this paper[22] is in Table 5. The 2 following ratios are then calculated:

$$\mathcal{R}_{\eta_c} = \frac{\mathcal{B}(\eta_c \to K^+K^-\eta)}{\mathcal{B}(\eta_c \to K^+K^-\pi^0)} = 0.571 \pm 0.025 \pm 0.051;$$
$$\mathcal{R}_{\eta_c(2S)} = \frac{\mathcal{B}(\eta_{c(2S)} \to K^+K^-\eta)}{\mathcal{B}(\eta_{c(2S)} \to K^+K^-\pi^0)} = 0.82\ 4 \pm 0.21 \pm 0.27.$$

The first ratio is in agreement with previous BES III result[25], but now the measurement is much more precise. Presence of non-negligible background in the η_c signals is found, which have different distributions in the Dalitz plot. A sideband subtraction is performed (yellow shaded histograms). Events in the tables are efficiency-weighted.

Table 4. Fitted η_c and $\eta_c(2S)$ parameters.

Resonance	Mass (MeV/c^2)	Γ (MeV)
$\eta_c \to K^+K^-\eta$	2984.1±1.1±2.1	34.8±4.0
$\eta_c \to K^+K^-\pi^0$	2979.8±0.8±3.5	25.2±2.4
$\eta_c(2S) \to K^+K^-\eta$	3635.1±5.8±2.1	11.3(fixed)
$\eta_c(2S) \to K^+K^-\pi^0$	3637.1±5.7±3.4	11.3 (fixed)

Table 5. Summary of the results from fits to $K^+K^-\eta$ and $K^+K^-\pi^0$.

Channel	Event yield	Ratio	Significance
$\eta_c \to K^+K^-\pi^0$	4518 ±131±50		32σ
$\eta_c \to K^+K^-\eta\,(\eta \to \gamma\gamma)$	853±38±11		21σ
$\mathcal{B}(\eta_c \to K^+K^-\eta)/\mathcal{B}(\eta_c \to K^+K^-\pi^0)$		0.602±0.032±0.065	
$\eta_c \to K^+K^-\eta\,(\eta \to \pi^+\pi^-\pi^0)$	292±20±7		14σ
$\mathcal{B}(\eta_c \to K^+K^-\eta)/\mathcal{B}(\eta_c \to K^+K^-\pi^0)$		0.523±0.040±0.083	
$\eta_c(2S) \to K^+K^-\pi^0)$	127±29±39		3.7σ
$\eta_c(2S) \to K^+K^-\eta)$	47±9±3		4.9σ
$\mathcal{B}(\eta_c \to K^+K^-\eta)/\mathcal{B}(\eta_c \to K^+K^-\pi^0)$		0.82±0.21±0.27	
$\chi_{c2} \to K^+K^-\pi^0$	88±27±23		2.5σ
$\chi_{c2} \to K^+K^-\eta$	2±5±2		0.0σ

The Dalitz analysis is then performed. The Dalitz plot of $\eta_c \to K^+K^-\eta$ and $\eta_c \to K^+K^-\pi^0$ are show in Fig. 9 and Fig. 10, respectively, with the projection of the invariant mass distributions and their unbinned maximum likelihood fit. A clear peak at the mass of $K_0^*(1430)$ is observed in both cases, together with other expected structures reported in Table 6 and 7, that shortly summarize the results of this search for the decay modes under exam. Amplitude parameterization is performed in a standard way for a pseudoscalar meson decaying to 3 pseudscalar mesons. Full interference is allowed among the amplitudes of all resonances in the Dalitz. No evidence for interferences between signal and background is found, so a sum of inchoerent resonances is used for fitting the sidebands. The non-resonant contribution is included in the fit. From our fit, we learn that the model provides an adeguate description of data for $\eta_c \to K^+K^-\eta$, while the isobar model does not describe properly the data for $\eta_c \to K^+K^-\pi^0$.

The third important contribution of this analysis is the determination of the $K_0^*(1430)$ parameters: scanning the likelihood as function of the $K_0^*(1430)$ mass and width, we obtain:

$$\mathrm{m}(K_0^*(1430)) = 1438 \pm 8 \pm 4\ \mathrm{MeV/c^2};$$
$$\Gamma(K_0^*(1430)) = 210 \pm 20 \pm 12\ \mathrm{MeV}.$$

This is the first observation of $K_0^*(1430) \to K\eta$. As this resonant state is observed in both samples, $\eta_c \to K^+K^-\eta$ and $\eta_c \to K^+K^-\pi^0$, we could measure the relative ratios:

$$f_{\eta K} = 0.164 \pm 0.042 \pm 0.010;$$
$$f_{\pi^0 K} = 0.338 \pm 0.019 \pm 0.004.$$

This allows to calculate:

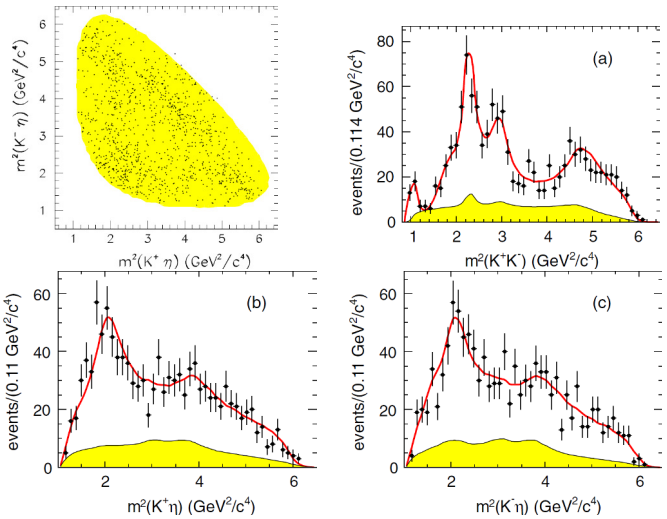

Figure 9. Dalitz plot of $\eta_c \to K^+K^-\eta$ (a) and Dalitz projection (b, c, d). The superimposed curves result from Dalitz plot analysis detailed described in Ref. [22]. The shades areas show the background estimates obtained by interpolating the results of the Dalitz plot analysis of the sideband regions.

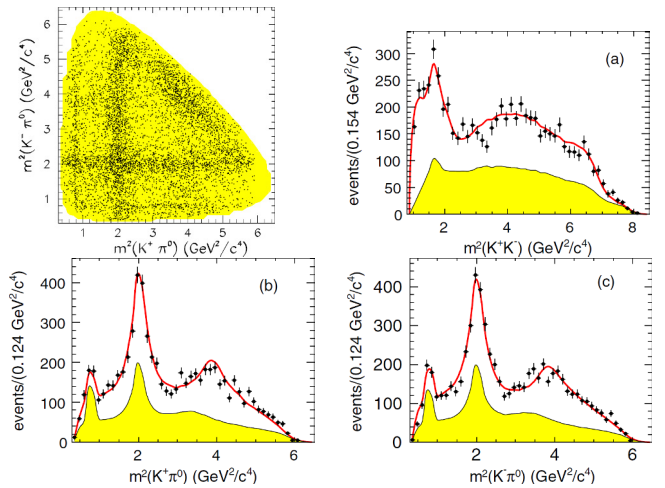

Figure 10. Dalitz plot of $\eta_c \to K^+K^-\pi^0$ (a) and Dalitz projection (b, c, d). The superimposed curves result from Dalitz plot analysis detailed described in Ref. [22]. The shades areas show the background estimates obtained by interpolating the results of the Dalitz plot analysis of the sideband regions

$$\frac{\mathcal{B}(K_0^*(1430)\to\eta K}{\mathcal{B}(K_0^*(1430)\to\pi^0 K} = \mathcal{R}(\eta_c)\cdot\frac{f_{\eta K}}{f_{\pi K}} = 0.092 \pm 0.025^{+0.010}_{0.025}.$$

In this work also the pseudoscalar meson mixing angle is evaluated: $\theta_P = (3.1^{+3.1}_{-5.0})^o$. It differs 2.9σ deviation from the results obtained from the $K_2^*(1430)$ ratio. This issue involves in theoretical discussions where the siglet and octet mixing angle should be considered separately.

Table 6. Results of the Dalitz plot analysis of $\eta_c \to K^+K^-\eta$.

Final state	Fraction %	Phase (radians)
$f_0(1500)\eta$	23.7±7.0±1.8	0.
$f_0(1710)\eta$	8.9±3.2±0.4	2.2±0.3±0.1
$K_0^*(1430)^+K^-$	16.4±4.2±1.0	2.3±0.2±0.1
$f_0(2200)\eta$	11.2±2.8±0.5	2.1±0.3±0.1
$K_0^*(1950)^+K^-$	2.1±1.3±0.2	-0.2±0.4±0.1
$f_2'(1525)\eta$	7.3±3.8±0.4	1.0±0.1±0.1
$f_0(1350)\eta$	5.0±3.7±0.5	0.9±0.2±0.1
$f_0(980)\eta$	10.4±3.0±0.5	-0.3±0.3±0.1
Non Resonant	15.5±6.9±1.0	-1.2±0.4±0.1
Sum	100.0±11.2±2.5	
χ^2/ν		87/65

Table 7. Results of the Dalitz plot analysis of $\eta_c \to K^+K^-\pi^0$.

Final state	Fraction %	Phase (radians)
$K_0^*(1430)^+K^-$	33.8±1.9±0.4	0.
$K_0^*(1950)^+K^-$	6.7±1.0±0.3	-0.67±0.07±0.03
$a_0(980)\pi^0$	1.9±0.1±0.2	0.38±0.24±0.02
$a_0(1450)\pi^0$	10.0±2.4±0.8	-2.4±0.05±0.03
$a_2(1320)\pi^0$	2.1±0.1±0.2	0.77±0.20±0.04
$K_2^*(1430)^+K^-$	6.8±1.4±0.3	-1.67±0.07±0.03
Non Resonant	124.4±2.5±0.6	1.49±0.07±0.03
Sum	85.8±3.6±1.2	
χ^2/ν		212/130

3 Bottomonium

The last part of this report is shortly dedicated to the radiative Υ(nS) transitions. They are generally well predicted from theoretical models[26]. *BABAR* collected a data sample of 14 fb^{-1} data at Υ(2S), and 28 fb^{-1} data at Υ(3S). With this data samples, to study the transitions $3S \to 2P \to 1S$, $3S \to 1P \to 1S$ and $2S \to 1P \to 1S$, to search for resonant χ_{bJ} states, is possible. Two are the samples available for this study: one involving one photon from the calorimeter and one from conversion e^+e^-, one with 2 calorimeter photons. Results are preliminary and the work is still in progress. However, in *BABAR* we have obtained the best evidence for the χ_{bJ}, J = 0, 1, 2.

4 Summary

In summary, recent original contributions are shown with the full *BABAR* dataset in the fields of charmonium and bottomonium physics. We observe signal for the decays $B^+ \to J/\psi K^+K^-K^+$, $B^0 \to J/\psi K^+K^-K_S^0$, $B^+ \to J/\psi\phi K^+$ and $B^0 \to J/\psi\phi K_S^0$, obtaining currently the most precise BF measurements. We search for resonance production in the $J/\psi\phi$ mass spectrum and obtain significances below 2σ for both the $X(4140)$ and the $X(4270)$ resonances, within systematic uncertainties. Limits on the BF of these resonances are obtained. We find that the hypothesis that the events are distributed uniformly on the Dalitz plot gives a poorer description of the data. We also search for

$B^0 \to J/\psi\phi$ and derive an UL on the BF for this decay mode, which is in agreement with theoretical expectations.

We have studied the processes $\gamma\gamma \to K^+K^-\eta/\pi^0$, and found the first observation of $\eta_c \to K^+K^-\eta$ decay, measuring its BF and performing for the first time a Dalitz analysis for each decay mode. The Dalitz analysis demonstrated the dominance of quasi-two-body amplitudes involving scalar-meson resonances. Under the hypothesis of a gluonium content in those, similar decay BFs to $\pi\pi$ and KK are expected. The first observation of $K_0^*(1430) \to K\eta$ was shown, with its relative BF. The result is not in full agreement with SU(3) expectation. We observed also $\eta_c(2S) \to K^+K^-\pi^0$ and give the first evidence for $\eta_c(2S) \to K^+K^-\eta$. The first evidence for the χ_{bJ} states is also introduced in this report.

References

[1] N. Brambilla *et all*, *Yellow Report*, hep-ph/0412158 (2005);

[2] Barnes and Godfrey, PRD **69**, 054008 (2004); Eichten, Lane and Quigg, PRD **69**, 094019 (2004); Swanson, PLB **588**, 189 (2004); Tornqvist, PLB **590**, 209 (2004); Suzuki, PRD **72**, 114013 (2005); Maiani, *et all*, PRD **71**, 014028 (2005).

[3] B. Aubert *et all* (*BABAR* Coll.), Phys. Rev. D. **71**, 071103 (2005); Phys. Rev. D **77**, 111101 (2008); Phys. Rev. D. **73**, 011101 (2006).

[4] S.K. Choi *et all* (*Belle* Coll.), Phys. Rev. Lett. **91**, 262001 (2003);

[5] B. Aubert *et all* (*BABAR* Coll.), Phys. Rev. Lett. **95**, 142001 (2005);

[6] T. Aaltonen *et all* (CDF Coll.), Phys. Rev. Lett. **102**, 242002 (2009); T. Aaltonen *et all* (CDF Coll.), hep-ex/1101.6058 (2011).

[7] B. Aubert *et all* (*BABAR* Coll.), Phys. Rev. Lett. **91**, 071801 (2003).

[8] A. Anastassov *et al.* (*CLEO* Coll.), Phys. Lett. B. **369**, 186 (1996) 360.

[9] BF calculations in Sec. 1 are performed using results from D. E. Groom *et al.*, the Particle Data Group Coll., *" Review of particle physics,"* Eur. Phys. J. C **15**, (2008). Update version: J. Beringer *et al.* (PDG Coll.), Phys. Rev. D **86**, 010001 (2012).

[10] S. Chatrchyan *et al.* (CMS Coll.), Phy. Lett. B **734**, 261 (2014).

[11] G. J. Feldman and R. D. Cousins, Phys. Rev. D. **57**, 3873 (1998).

[12] R. Aaij *et all* (LHCb Coll.), Phys. Rev. D **85**, 091103(R) (2012).

[13] J.P. Lees *et all* (BABAR Coll.), hep-ex/1407.7244 (2014).

[14] V.M. Abazov *et all* (D0 Coll.), Phys. Rev. D **89**, 012004 (2014).

[15] L. Kopke and N. Wermes, Phys. Rep. **174**, 67 (1989); J.Z. Bai *et all* (BES Coll.) Phys. Rev. D **68**, 052003 (2009).

[16] V. Mathieu, N. Kochelev and V. Vento, Int. J. Mod. E**18**, 1 (2009).

[17] G. S. Adams *et all* (CLEO Coll.) Phys. Rev. D **84**, 112009 (2011).

[18] C. Amsler and F. Close, Phys. Rev. D **53**, 295 (1996).

[19] J.P. Lees *et all* (BABAR Coll.) Phys. Rev. D **85**, 112010 (2012).

[20] X.-G. He and T.C. Yuan, hep-ph/0612108.

[21] D. Aston *et all* (LASS Coll.), Nucl Phys. **B296**, 493 (1988).

[22] J.P. Lees *et all* (*BABAR* Coll.), Phys. Rev. D **79**, 112004 (2014).

[23] B. Aubert *et all* (*BABAR* Coll.), Phys. Rev. D **79**, 112001 (2009).

[24] C.N. Yang, Phys. Rev. **77**, 242 (1950).

[25] M. Ablikim *et all* (BES III COll.), Phys. Rev. D **86**, 092009 (2012).

[26] R. Lewis and R. M. Woloshyn, Phys. Rev. D **84**, 094501 (2011).